

Supplementary Materials for

Frequency division using a soliton-injected semiconductor gain-switched frequency comb

Wenle Weng*, Aleksandra Kaszubowska-Anandarajah*, Junqiu Liu, Prince M. Anandarajah, Tobias J. Kippenberg*

*Corresponding author. Email: wenle.weng@epfl.ch (W.W.); anandara@tcd.ie (A.K.-A.); tobias.kippenberg@epfl.ch (T.J.K.)

Published 25 September 2020, *Sci. Adv.* **6**, eaba2807 (2020)
DOI: 10.1126/sciadv.aba2807

This PDF file includes:

Sections S1 to S5
Figs. S1 to S7
Table S1

S1 Natural lasing spectrum of the DFB laser

Figure S1 shows the CW lasing spectrum of the DFB laser without optical injection locking. Around the central lasing mode at 1546 nm, the side modes of the DFB structure are shown by the ripples on the spectrum background. The spacing of the side modes are approximately 1.6 nm. In the main text the soliton-injected GSL spectra in Figure 2 (b) show comb spectral ripples with a period of ~ 1.6 nm, which are attributed to the enhancement due to the DFB side modes. In addition, many other possible reasons, including spatial hole burning effect, birefringent effect, four wave mixing effect, the varied laser gain at different wavelengths, and some etalon effect due to the reflections from the multiple fiber ends and chip facets, can contribute to the overall spectral non-uniformity of the GSL combs. A thorough investigation of these effects is beyond the scope of this study.

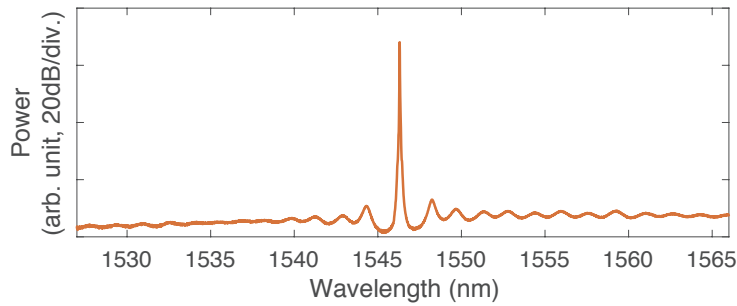


Figure S1: **Natural lasing (i. e., without gain switching or optical injection) spectrum of the DFB laser.** Besides the central lasing mode at 1546 nm, multiple longitudinal modes with a spacing of ~ 1.6 nm can be observed from the ripples in the background.

S2 Physical model of the soliton-injected gain-switched comb

The gain switching laser rate equations that couple the photon number $|A_{\text{GSL}}|^2$ in the laser's active volume and the carrier density N can be written as:

$$\frac{dA_{\text{GSL}}}{dt} = \frac{1}{2}(1 - i\alpha_{\text{H}})[aV(N - N_0) - \frac{1}{\tau_{\text{p}}}]A_{\text{GSL}} + \sqrt{\kappa_{\text{c}}}s_{\text{inj}} + F_{\text{E}} \quad (\text{S1})$$

$$\frac{dN}{dt} = \frac{I_{\text{bias}} + I_{\text{gs}} \sin(\omega_{\text{gs}} t + \Phi)}{eV} - (\gamma_1 N + \gamma_2 N^2 + \gamma_3 N^3) - a(N - N_0) \frac{|A_{\text{GSL}}|^2}{V} + F_N \quad (\text{S2})$$

where α_{H} is the linewidth enhancement factor, a is the differential gain, V is the laser active volume, N_0 is the carrier density at transparency, κ_c is the injection coupling rate, and $|s_{\text{inj}}|^2 = \frac{P_{\text{inj}}}{\hbar\omega_0}$ is the injected photon flux, with P_{inj} being the injected power. The carrier recombination rate is represented by $\gamma_1 N + \gamma_2 N^2 + \gamma_3 N^3$, showing the combined effects of non-radiative recombination, the radiative recombination and the Auger recombination. To implement gain switching operation, the gain-switching current I_{gs} modulated at frequency ω_{gs} is added to the biased current I_{bias} . The elementary charge is denoted by e . A relative phase Φ , which is adjusted to obtain error signals with high contrast, is added into the modulation term. Practically the relative phase between the gain-switching current and the injected DKS can be tuned by adjusting the polarization controller in Fig. 2 (a) in the main text or by tuning the phase of the gain switching signal with the driving signal generator. The spontaneous emission into the lasing field and the stochastic carrier recombination are denoted by the Langevin noise terms F_E and F_N respectively, with $F_E = \sqrt{\beta\gamma_2 N^2 V B_{\text{sim}}}(e_I(t) + ie_Q(t))$ and $F_N = \sqrt{2(\gamma_1 N + \gamma_2 N^2 + \gamma_3 N^3) B_{\text{sim}}/V} e_N(t)$. Here β is a factor related to the amount of spontaneous emission into the lasing mode, and B_{sim} is the simulation bandwidth. The stochastic unit Gaussian random variable noise terms e_N , e_I and e_Q have zero mean value and unity variance. Note that for the optical field both the in-phase component e_I and the quadrature component e_Q are included in the spontaneous emission effect.

First we perform simulation without the injection term $\sqrt{\kappa_c} s_{\text{inj}}$. The gain switching frequency is set to be 7 GHz. The values of other parameters used in the simulation are presented in Table S1. Figure S2 shows the optical spectrum and the GSL output intensity profile. Because of the stochastic terms, without injected master laser field, the GSL pulses have incoherent phases that result in the spectrum in Fig S2 (a), which shows noisy floor and unresolvable comb teeth. We also measure the GSL spectrum experimentally with an optical spectrum analyzer (OSA) with a measurement resolution of 0.2 nm. Again, due to the incoherent emission, the

Symbol	Value	Unit	Definition
α_H	3		Linewidth enhancement factor
a	1.33×10^4	s^{-1}	Differential gain
N_0	1×10^{24}	m^{-3}	Carrier density at transparency
τ_P	3	ps	Photon lifetime
k_c	2.4×10^6	s^{-1}	Injection coupling factor
I_{bias}	50	mA	Biased current
I_{gs}	50	mA	Gain switching current
γ_1	1×10^9	s^{-1}	Non-radiative recombination rate
γ_2	1×10^{-16}	$s^{-1}m^3$	Radiative recombination coefficient
γ_3	1×10^{-41}	$s^{-1}m^6$	Auger recombination coefficient
V	6×10^{-17}	m^3	Volume of active section
β	5×10^{-4}		Fraction of spontaneous emission into lasing mode
e	1.6×10^{-19}	C	Elementary electronic charge
B_{sim}	$14 \times 10^9 \times 2^8$	Hz	Simulation bandwidth
D_1	$14 \times 10^9 \times 2\pi$	rad	first-order dispersion coefficient
D_2	$2 \times 10^3 \times 2\pi$	rad	Second-order dispersion coefficient
κ	$200 \times 10^3 \times 2\pi$	rad	Loaded loss rate
κ_{ex}	$100 \times 10^3 \times 2\pi$	rad	External coupling rate
P_{in}	0.12	W	Pump power
n_2	9×10^{-21}	m^2/W	Kerr nonlinear index
n	1.37		Material refractive index
V_0	2.5×10^{-12}	m^3	Effective mode volume
ω_0	$1.934 \times 10^{14} \times 2\pi$	rad	Pumped mode angular resonance frequency
ω_p	$\omega_0 - 6 \times 10^6 \times 2\pi$	rad	Pump laser angular frequency

Table S1: Values and definitions of parameters used in simulations. In the first block are the parameters for of the gain-switched laser. The second block contains parameters used for the LLE model.

OSA cannot resolve any frequency comb teeth.

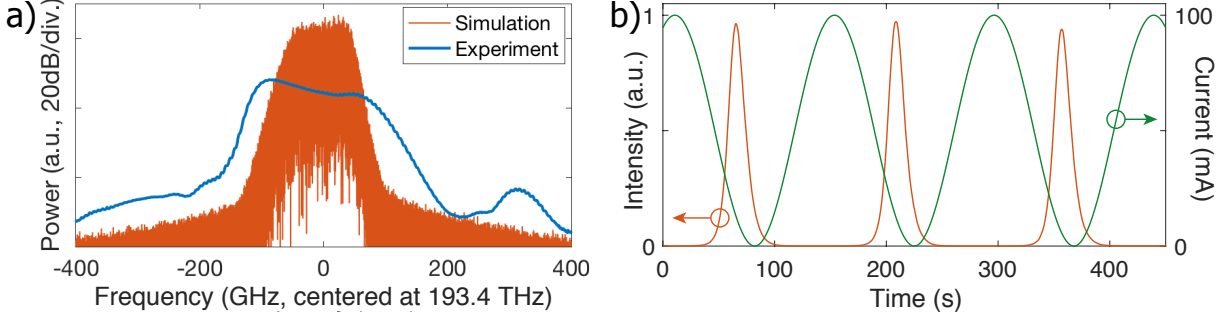


Figure S2: **Gain-switched laser without injection.** (a) The experimental and simulated optical spectra of the GSL. (b) The simulated output intensity of the GSL. The green trace is the modulated current.

To prepare the soliton microcomb field for the injection locking, we use a modified model based on the Lugiato-Lefever equation. The model contains pump laser phase and amplitude noises as well as frequency noise added to the pump-resonance detuning:

$$\frac{\partial A}{\partial t} - i\frac{1}{2}D_2\frac{\partial^2 A}{\partial \phi^2} - ig|A|^2A = \left(-\frac{\kappa}{2} + i(\omega_0 - \omega_p + \zeta_\omega(t))\right)A + \sqrt{\kappa_{\text{ex}}} \cdot (s_{\text{in}} + \zeta_{\text{amp}}(\phi, t)) \cdot e^{i\zeta_{\text{pha}}(\phi, t)} \quad (\text{S3})$$

In this model $|A|^2$ is the intracavity photon number and A can be viewed as the envelope of the intracavity field, ϕ is the angular coordinate in the co-rotating frame that is related to the round-trip fast time coordinate τ by $\phi = \tau \times D_1$ (where $\frac{D_1}{2\pi}$ is the FSR), κ is the cavity decay rate, κ_{ex} is the external coupling rate, and $|s_{\text{in}}|^2 = \frac{P_{\text{in}}}{\hbar\omega_0}$ is the driving photon flux, where P_{in} is the power of the main pump. Here $g = \frac{\hbar\omega_0^2 cn_2}{n^2 V_0}$ is the single photon induced Kerr frequency shift, where n and n_2 are the refractive and nonlinear optical indices, V_0 is the effective mode volume, and c is the speed of light. Since both the MgF₂ resonator and the Si₃N₄ microring resonator have very small third-order dispersions, only the second-order dispersion coefficient D_2 is included in the simulation. The Gaussian noise terms $\zeta_\omega(t)$, $\zeta_{\text{amp}}(\phi, t)$ and $\zeta_{\text{pha}}(\phi, t)$ have zero mean value and variances of $200 \times 2\pi$ radian, 0.01 and 0.01 respectively, representing the detuning frequency noise, the laser amplitude noise and the laser phase noise, respectively. Other parameters used

in the simulation are shown in Table S1. We simulate for consecutively 1×10^4 round-trip times with single-soliton state. The soliton microcomb spectrum (with CW background removed) computed with the simulated soliton field is shown in the upper panel in Fig. S3 (a), while the soliton intensity profiles in the time domain are displayed in the upper panel in Fig. S3 (b).

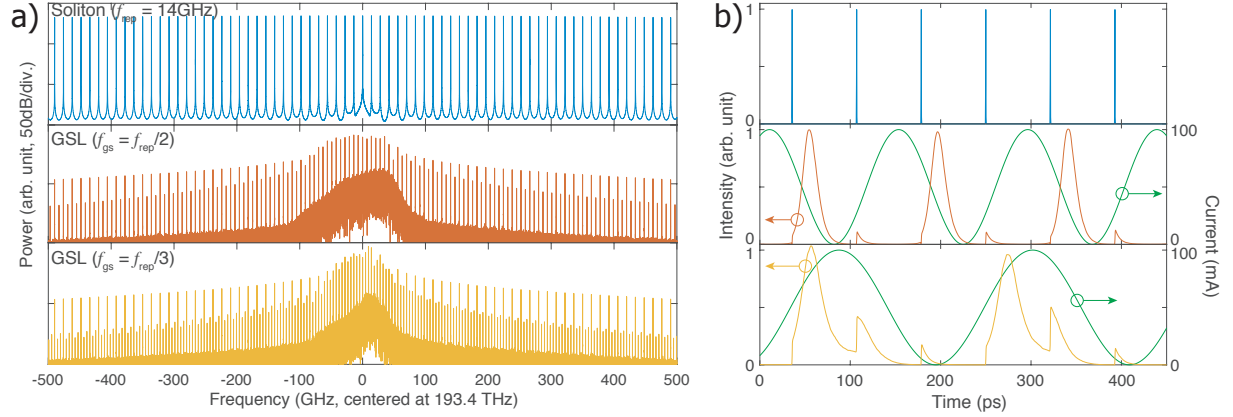


Figure S3: Simulation of a soliton-injected gain-switched comb. (a) The numerically simulated comb spectra of the soliton microcomb with $f_{\text{rep}} = 14$ GHz used for injection (upper panel), the gain-switched comb with $f_{\text{gs}} = f_{\text{rep}}/2$ (middle panel), and the gain-switched comb with $f_{\text{gs}} = f_{\text{rep}}/3$ (lower panel). (b) The corresponding comb intensity profiles in the time domain. The applied gain switching current is also shown by the green traces.

To simulate the GSL dynamics with soliton injection, the CW background contained in A is removed. Then $s_{\text{inj}} = \eta A e^{-i\omega' t}$ is inserted into Eq. S1 to numerically integrate the coupled equations, with η being a factor to make the average power of E_{inj} to be 5 mW, and ω' being the carrier angular frequency difference between the DKS and the GSL without injection. Here we use $\omega' = 0.5 \times 10^9 \times 2\pi$ for the simulation. We note here that the injection locking can be achieved with much larger ω' values, even when it is larger than the cavity FSR. The relative phase between the applied gain switching current and the injected soliton field is adjusted to obtain relatively low intensity fluctuations of the GSL. The middle and the lower panels in Fig. S3 show the simulated GSL spectra and the intensity profiles at two different gain switching frequencies. The overall results show satisfying qualitative agreement with the experimental

results presented in the main text. From the time domain profiles it is clear that the injected solitons initiated GSL pulses at the suitable gain switching current levels. Therefore the output GSL pulses have highly coherent phases which are disciplined by the soliton microcomb. One can see that the simulated GSL spectra feature highly resolvable comb teeth that are at least 30 dB above the noise floor, showing the dramatically improved coherence.

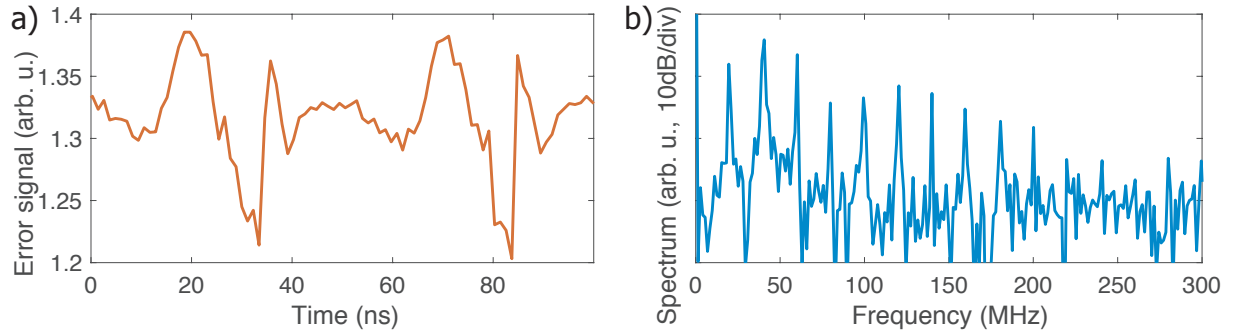


Figure S4: **Simulated error signal and gain-switched laser power spectrum.** (a) The simulated laser intensity. A frequency offset of 10 MHz is added to f_{gs} to have the relation of $2 \times f_{gs} - f_{rep} = 20$ MHz. (b) The power spectrum calculated by applying fast Fourier transform to the simulated error signal.

In Fig. S4 (a) we show the simulated time domain GSL power fluctuations at the frequencies below 1 GHz when we deliberately add a frequency offset to the 7 GHz gain switching frequency to simulate the situation with imperfect frequency division (e. g., subharmonic locking is off). The power fluctuations are similar to the error signals generated by PD2 in the experiment, with comparable relative contrast and shapes. Figure S4 (b) shows the spectrum of the fluctuations, which is also in good agreement with the experimental spectrum shown in Fig. 2 (d) in the main text. This result validates the mechanism of the subharmonic locking, showing that the error signals have fine contrast and quality, which are the foundations of a robust SPL.

S3 Heterodyne beatnote of beating combs with a reference laser

To confirm the comb nature of the injection-locked GSL, we beat the DKS microcomb and the GSL comb ($f_{\text{gs}} = f_{\text{rep}}/2$) with a 1553-nm reference laser that is frequency locked to an ultrastable cavity. Figure S5 (a) shows the comb spectra and the reference laser emission. The beat signals that are generated by a high-bandwidth photodetector are measured by an electrical spectrum analyzer (ESA). Figure S5 (b) shows the beat signals. Beating between the DKS microcomb and the reference laser produces a beat signal at 6.23 GHz. When beating the GSL comb with the reference laser, two signals at 6.23 GHz and 0.82 GHz are detected within the detection bandwidth of 7 GHz, corresponding to a GSL comb tooth that is seeded by the DKS comb and a sideband tooth that divides f_{rep} , respectively. On the right hand side of Fig. S5 (b) are the detailed spectra of the three beat signals denoted by numbers. The resolution bandwidth is 1 kHz. The sidebands around the central signals are caused by the PDH modulation frequency of 387 kHz that is applied on the reference laser. All the three signals exhibit almost identical linewidths, confirming that the GSL comb indeed yields perfect repetition rate division and that the coherence of the injected DKS microcomb is well kept in the GSL comb.

S4 Long-term repetition rate frequency stability

Frequency division of a DKS microcomb's repetition rate f_{rep} with GSL offers an approach to measure and to stabilize the DKS frequency, even if f_{rep} is too high to be directly measured with conventional electronics. The experimental setup illustrated in Fig. 2 (a) in the main text uses the correction signal that enables the subharmonic phase locking as an error signal for stabilization of the DKS microcomb. The error signal is generated by the SPL servo output that enforces f_{gs} to follow f_{rep} , therefore stabilizing this signal with pump power control stabilizes f_{rep} . Figure S6 (a) presents the frequency drifts of f_{rep} of the MgF₂ microresonator soliton microcomb. The

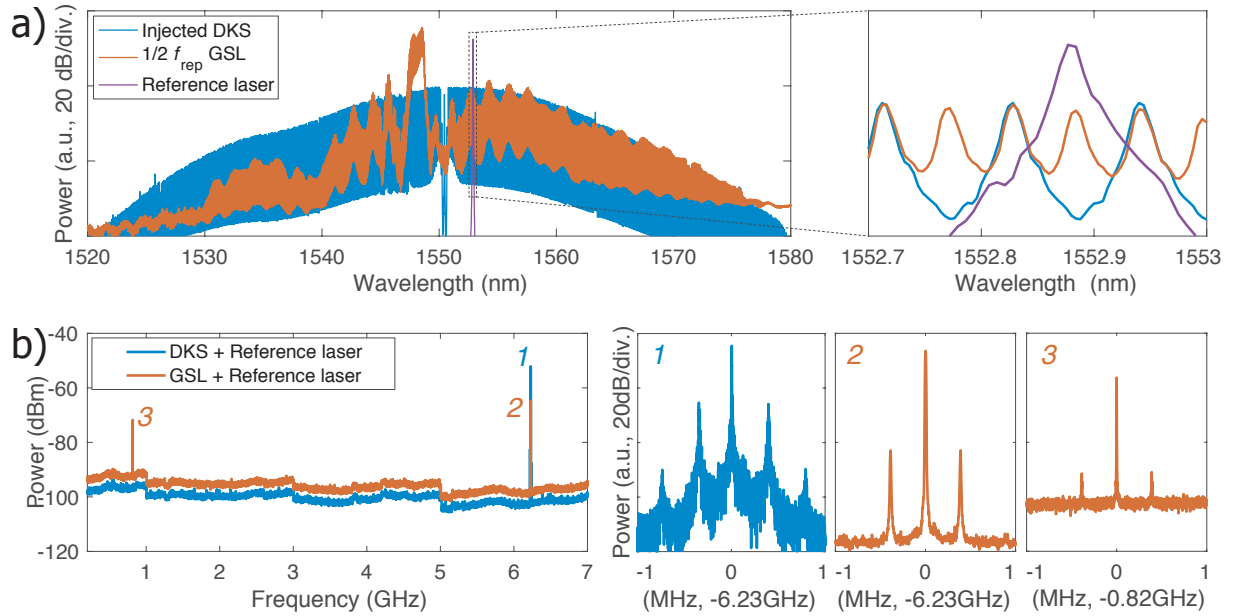


Figure S5: Beating the soliton microcomb and the gain-switched comb with a reference laser. (a) Optical spectra of the frequency combs and the reference laser. The figure on the right hand side shows the detailed spectra from 1552.7 nm to 1553 nm. (b) The beat signals measured by an ESA. The signals are denoted by numbers. On the right hand side are the corresponding detailed spectra (RBW = 1 kHz) of the signals.

repetition rate around 14.093 GHz was detected by a fast photodetector, and then divided by a factor of 16 with an electronic frequency divider. The divided frequency was measured by a frequency counter with a gate time of 0.1 s. In Fig. S6 (b) are the relative Allan deviations of the frequency drifts. This measurement shows that the pump power control suppresses f_{rep} fluctuations, improving the long-term frequency stability of the soliton microcomb by more than one order of magnitude. One should note that the stabilization ability is currently limited by the slow response time of the thermal actuation. Considerable improvement should be expected with faster actuation techniques such as mechanical control via piezo actuation.

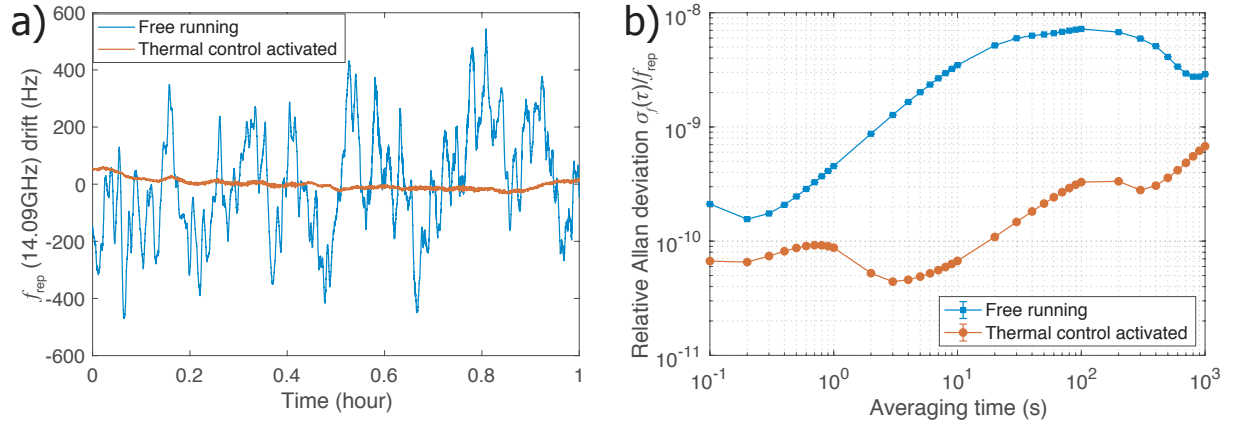


Figure S6: **Soliton microcomb repetition rate frequency stabilities.** (a) The frequency drifts of the 14.093-GHz repetition rate when the thermal control via pump power modulation is off (blue trace) and on (red trace). A electronic frequency divider ($\div 16$) and a frequency counter with gate time of 0.1 s were used to make the measurement. (b) Computed relative Allan deviations of the repetition rate fluctuations. The error bars are barely visible in the figure due to their small values.

S5 Frequency multiplication of the repetition rate of a mode-locked laser

The pulse-injection-locking technique developed in this work not only allows us to perform frequency division of the repetition rate of a pulse train, but also provides a new approach for frequency multiplication of a pulse train's repetition rate if the repetition rate is relatively low. To demonstrate the concept, we replace the DKS microcomb with a mode-locked laser (MLL) optical frequency comb (OFC) whose repetition rate is approximately 250 MHz. Figure S7 (a) shows the experimental setup. An optical bandpass filter (BPF) is used to filter the MLL-OFC output so that only a 5-nm-wide comb spectrum with the power of a few milliwatts is sent into the GSL. We apply f_{gs} around 5 and 10 GHz respectively, which correspond to a multiplication factor of $n = 19$ and $n = 38$, respectively. Error signals similar to those in the frequency division experiment are produced by the photodetector, allowing us to actively lock the signal generator's frequency to be a multiplication of the repetition rate of the MLL. Figure S7 (b) shows the spectra of the injected MLL and the harmonically phase locked GSL of $n = 38$

($f_{\text{gs}} = 9.56$ GHz). While the resolution of the OSA is not able to resolve the teeth of the MLL-OFC due to the low repetition rate, the GSL spectrum does not show any comb teeth either, which suggests that the GSL does not possess pulse-to-pulse coherence. Next, we measure the phase noise levels of the MLL repetition rate and the frequency-multiplied microwaves. The results are presented in Fig. S7 (c). The servo control bandwidth can be seen from the spikes around 40 kHz in the phase noise spectra of the synthesized microwaves. Within this control bandwidth, the rises of the phase noise levels are in excellent agreement with the multiplication factors. We also measure the power spectra of the GSL output (see Fig. S7 (d) and (e)). The dominant signals at f_{gs} and the weak signals at the MLL f_{rep} and its harmonics are observed, clearly showing the multiplication factors.

While the demonstrated results show that the frequency multiplication scheme is highly effective, one can notice, based on the optical spectra in Fig. S7 (b), that a key feature that is distinct from the frequency division scheme is the loss of GSL pulse-to-pulse coherence. To confirm this feature, we use a 1549-nm CW laser to beat with the GSL. The beat signal spectrum is displayed in Fig. S7 (f). In the spectrum, in every 251.6-MHz frequency division separated by the MLL f_{rep} and its harmonics there are two weak signals generated by the beating between the CW laser and the weak MLL components contained in the GSL. However, within the frequency range from dc to $f_{\text{gs}} = 4.78$ GHz we do not observe two strong beat signals, which would appear if the GSL output is a coherent frequency comb. This result is in agreement with the optical spectra measurement, showing that the GSL does not exhibit pulse-to-pulse coherence, despite the high stability of the pulse repetition rate. This phenomenon can be intuitively understood when one considers that the phase of any GSL pulse is determined only when it is seeded by the injected DKS/MLL pulses. In the frequency division scheme, since every GSL pulse is seeded by the DKS pulses multiple (n) times, the GSL pulse train is highly coherent. Contrastingly, in the frequency multiplication scheme, only one in every n GSL pulses is seeded by one MLL

pulse. As a result, no pulse-to-pulse coherence can be obtained because the phases of the $n - 1$ unseeded pulses are totally random, being initiated by the semiconductor laser spontaneous emission.

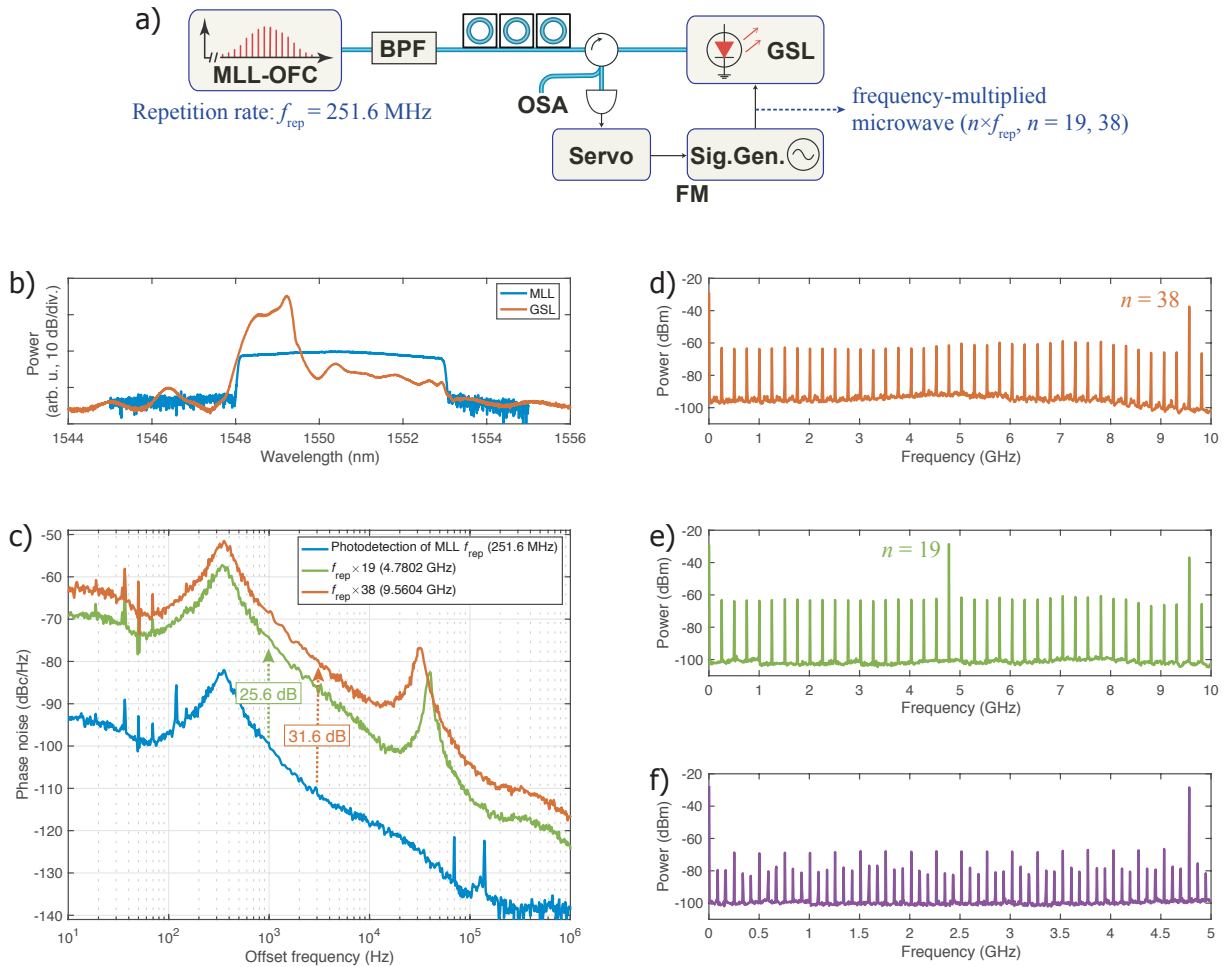


Figure S7: Frequency multiplication using optical injection from a mode-locked laser. (a) The experimental setup. BPF: optical bandpass filter. (b) Optical spectra of the mode-locked laser and the injection-locked GSL. (c) Phase noise spectra of the repetition rate of the mode-locked laser and the synthesized frequency-multiplied microwaves. (d) The power spectrum of the injection-locked GSL with $n = 38$. (e) The power spectrum of the injection-locked GSL with $n = 19$. (f) The heterodyne beat signal spectrum of the injection-locked GSL with $n = 19$.